A model for large-scale volcanic plumes on Io: Implications for eruption rates and interactions between magmas and near-surface volatiles

Enzo Cataldo, Lionel Wilson, Steve Lane, and Jennie Gilbert

Department of Environmental Science, Institute of Environmental and Natural Sciences, Lancaster University, Lancaster, UK

[1]   Volcanic plumes deposit magmatic pyroclasts and SO_2 frost on the surface of Io. We model the plume activity detected by Galileo at the Pillan and Pele sites from 1996 to 1997 assuming that magmatic eruptions incorporate liquid SO_2 from near-surface aquifers intersecting the conduit system and that the SO_2 eventually forms a solid condensate on the ground. The temperature and pressure at which deposition of solid SO_2 commences in the Ionian environment and the radial distance from the volcanic vent at which this process appears to occur on the surface are used together with observed vertical heights of plumes to constrain eruption conditions. The temperature, pressure, and density of the gas–magma mixtures are related to distance from the vent using continuity and conservation of energy. Similar eruption mass fluxes of order $5 \times 10^7 \, kg \, s^{-1}$ are found for both the Pillan and the Pele plumes. The Pele plume requires a larger amount of incorporated SO_2 (29–34 mass %) than the Pillan plume (up to ~6 mass %). Implied vent diameters range from ~90 m at Pillan to ~500 m at Pele. The radial extents of the optically dense, isothermal, incandescent parts of the eruption plumes immediately above the vents are ~100 m at Pillan and ~1300 m at Pele. Gas pressures in the vents are ~20 kPa at Pillan and ~2 kPa at Pele and the eruption conditions appear to be supersonic in both cases, though only just so at Pele.   *INDEX TERMS:* 8450 Volcanology: Planetary volcanism (5480); 8414 Volcanology: Eruption mechanisms; 6218 Planetology: Solar System Objects: Jovian satellites; 5470 Planetology: Solid Surface Planets: Surface materials and properties; 6061 Planetology: Comets and Small Bodies: Remote sensing; *KEYWORDS:* Io, explosive volcanism, volatiles, plumes, eruption rates

1.   Introduction

[2]   On Io, volcanic plumes are common. They appear to be mainly driven by SO_2 gas along with minor concentrations of sulfur and probably other sulfur compounds [*Smith et al.*, 1979; *McEwen and Soderblom*, 1983; *Johnson et al.*, 1995; *Lopes-Gautier et al.*, 2000]. The instruments aboard the Galileo spacecraft have confirmed the existence of SO_2 within both the Pillan and Pele plumes [*McEwen et al.*, 1998a] which are the subjects of this investigation (Figures 1a and 1b). Recently, sulfur dioxide deposits have been mapped at scales of less than 10 km, revealing a more complex relationship to surface colors, and some red areas, previously thought to be depleted in SO_2, now reveal its existence [*Lopes-Gautier et al.*, 2000]. After the 5 month-long eruption at Pillan first imaged on 28 June 1997, a new 400 km diameter circular plume fall deposit, dark at all observed wavelengths, formed around Pillan Patera [*McEwen et al.*, 1998a]. This deposit appears to be similar to the dark fan-shaped deposit, 200 km in radial extent, extending outward from the Pele volcanic center [*Strom and Schneider*, 1982]. Further away from the Pele vent, red annular deposits are found, whereas no evidence for surface condensates is seen at Pillan [*McEwen et al.*, 1998a]. However, a process of SO_2 condensation within the Pillan plume has been suggested by Hubble Space Telescope (HST) and ground-based observations [*Spencer et al.*, 1997a].

[3]   Conversion of atmospheric water vapor to liquid droplets or hailstones, micrometer to submillimeter in size, is an important process in terrestrial volcanic plumes [*Rogers and Yau*, 1989]. Available ash particles or particle aggregates act as condensation nuclei and may spend a substantial part of their airborne lifetime coated with liquid or solid condensate [*Gilbert and Lane*, 1994]. The occurrence of liquid water at low relative humidities and at temperatures less than 0°C is probably due to the presence of sulfuric acid [*Ammann and Burtscher*, 1993]. The covering of particles or particle aggregates by ice occurs when they are convected upwards through the atmosphere to very-low-temperature regions.

[4]   Evidence for condensates on individual glassy volcanic particles was also found in some lunar soils sampled during two lunar Apollo missions (15 and 17). These soils were dominated by droplets of volcanic glass, averaging
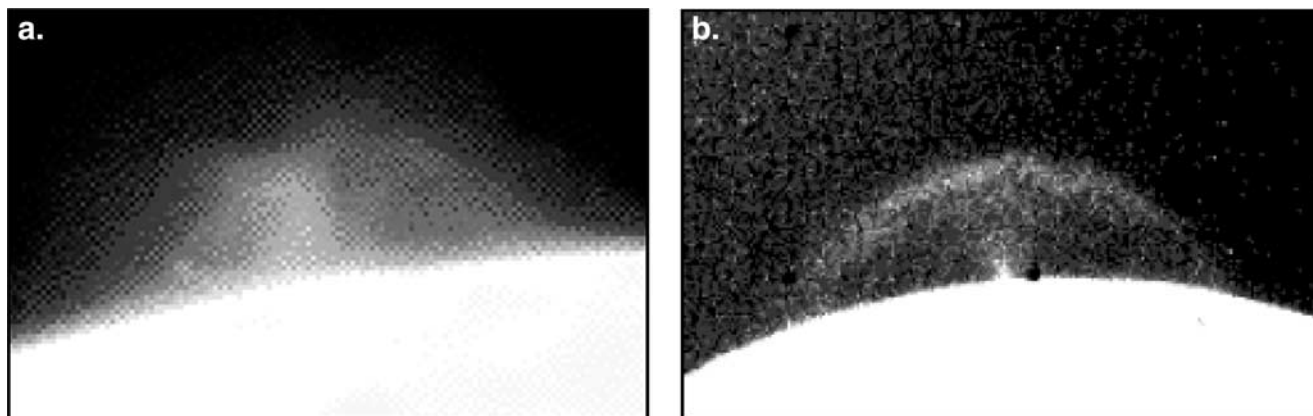
Figure 1. (a) Galileo SSI image of the Pillan eruption plume. Image width is 645 km (frame 401863203, violet filter, orbit C9, 28 July 1997, resolution 12 km pixel^{-1}). (b) Voyager 1 image of the Pele eruption plume. Image width is 1425 km (frame FDS 16368.50, ultraviolet filter, 4 March 1979, resolution 7.3 km pixel^{-1}).

~0.1–0.3 mm diameter [*Gibson and Moore*, 1973a, 1973b]. Various volatile elements (e.g., Zn, Ga, Pb, Cu, Tl, S, F, and Cl) appeared to be concentrated in surficial deposits on both the Apollo 15 and 17 glass spherules [*Gibson and Moore*, 1973a, 1973b; *Chou et al.*, 1975; *Meyer et al.*, 1975; *Wasson et al.*, 1976; *Butler*, 1978]. The same authors concluded that these elements condensed on the outside surface of the glassy particles in lava fountains.

[5] Previous models of explosive volcanic eruptions on Io, although addressing many aspects of the fluid mechanics of the discharge of gas or gas–particle mixtures into a vacuum [e.g., *Cook et al.*, 1979; *Smith et al.*, 1979; *Strom et al.*, 1979; *Collins*, 1981; *Wilson and Head*, 1981a; 2001; *Kieffer*, 1982, 1984; *Strom and Schneider*, 1982; *James and Wilson*, 1998; *Cataldo and Wilson*, 2000; *Kieffer et al.*, 2000; *Glaze and Baloga*, 2000], have generally not dealt in great detail with the dynamic interactions between volatiles and pyroclasts. Here we present a simple fluid-dynamic and thermodynamic model of explosive volcanic eruptions on Io which includes such interactions, and in which the eruption conditions are constrained by considering the distances from the vent at which SO_2 gas in plumes is deposited directly as a solid onto the ground.

2. Model Assumptions and Initial Conditions

2.1. Steady Eruptions of Gas and Magma

[6] We start by considering steady eruptions of gas and magma at the Pillan and Pele sites, both locations being associated with very-high-temperature hot spots [*McEwen et al.*, 1998b]. The steady assumption is justified by the duration, at least a few months, of most volcanic events observed by both the Voyager and Galileo imaging systems [*Strom and Schneider*, 1982; *McEwen et al.*, 1998a]. The earliest stages of an eruption on Io are likely to involve choked flow, in which the conduit near the surface does not flare sufficiently rapidly to allow a transition from subsonic to supersonic flow to occur below the surface [*Kieffer*, 1982]. The exit pressure at the surface vent is much greater than the ambient pressure

(a near-vacuum on Io, no more than 10^{-1} Pa near plumes and 10^{-3} Pa elsewhere) [*Lellouche*, 1996; *Spencer et al.*, 2000], the eruption speed is limited to be equal to the speed of sound in the mixture of gas and particles exiting the vent, and a system of shocks in and above the vent allows the pressure to decrease and the magma eruption speed to increase to equilibrium values [*Kieffer*, 1984]. However, accumulation of pyroclasts around the vent and erosion of the vent walls may together allow the vent shape to adjust itself toward that of a De Lavalle nozzle, the profile of which allows a smooth transition to pressure balanced flow [*Wilson and Head*, 1981b], i.e., flow in which the pressure at any given depth is not too greatly different from the lithostatic pressure in the crustal rocks, so that there are minimal stresses across the walls of the conduit. This process is most likely to occur in a long-lived eruption, and would lead to pyroclasts leaving the vent region with a wide range of elevation angles, from 90° (vertical) to 45° (leading to the maximum range if planetary surface curvature is neglected) to some small value dictated by the exact vent geometry. We assume that this wide range of elevations is present in the eruptions we model and, for simplicity, also assume that equal numbers of pyroclasts are ejected at all elevations and azimuths.

2.2. Interaction Between Magma and Liquid SO_2 at Shallow Depths

[7] The erupting magma, with a maximum temperature up to 1900 K, consistent with Galileo hot spot data [*McEwen et al.*, 1998a, 1998b], is assumed to interact with SO_2, which will become a liquid at the temperature and pressure relevant to a depth of 1.75 km and a supercritical fluid at depths greater than ~2 km (see phase diagram in the work of *Kieffer et al.* [2000]). Such an assumption is consistent with current models of the Ionian crust, which favor a silicate makeup with a substantial amount of SO_2 deposits concentrated at its uppermost layers [*Keszthelyi and McEwen*, 1997; *Kieffer et al.*, 2000]. We start from the *Wohletz* [1986] approach to magma–water interactions, in which magma and external water are allowed to mix intimately and come close to thermal equilibrium before

significant explosive expansion may occur. During a steady eruption, the injection of a volatile liquid from an aquifer through the conduit walls will occur over a finite range of depths. Intimate mingling, which will be most effective after the magma has disrupted into liquid droplets entrained in the gas stream, will bring the system to a thermal and dynamic equilibrium. Assuming that all of the liquid is vaporized, the redistribution of thermal energy as the magma cools and the entrained SO_2 is converted to vapor and heated leads to:

$$(1 - n)(T_{mi} - T)C_m = n[L_s + (T_b - T_1)C_{sl}] + (T - T_b)C_{sv}, \quad (1)$$

where n is the mass fraction of liquid SO_2 added to the magma, T_{mi} is the initial magma temperature, T is the equilibrium temperature after mixing, C_m is the specific heat of the magma, L_s and T_b are the latent heat of vaporization and the boiling point of SO_2 (262.4 K), respectively, T_1 is the temperature of the SO_2 liquid (taken as 200 K), and C_{sl} and C_{sv} are the specific heats of liquid and gaseous SO_2, respectively. The relationship thus obtained relates the SO_2 mass fraction and temperature of the mixture of magma and SO_2 emerging from the vent: the higher the mass proportion of incorporated SO_2 (we assume that values up to at least 30 mass % are possible), the lower the temperature.

2.3. The Optically Thick Portions of the Plumes

[8] We assume that a zone exists, extending a few kilometers radially outward from the Pillan and Pele vents, within which the number density of magma droplets/pyroclasts is so high that the plume is optically dense (i.e., opaque to the transmission of thermal radiation) [*Wilson and Head*, 1981b]. Essentially zero heat is lost, thus buffering the temperature, while the pressure varies in accordance with a continuity equation. We cannot observe this region directly at Pele or Pillan because no suitably oriented images of the plumes were obtained at high enough spatial resolution (Pillan has not been active since November 1997 and limb images taken by Galileo prior to this have resolutions no better than ~8 km pixel^{-1} [*McEwen et al.*, 1997b]; similarly the best limb images of Pele have resolutions ranging from 7 km pixel^{-1} (Voyager images) [*Strom et al.*, 1979] to ~14 km pixel^{-1} (Galileo) [*Davies et al.*, 2001]). However, the assumption now seems to be supported by some very-high-resolution (<1 km) images of an eruption issuing from a fissure vent in one of the calderas of the Tvashtar Catena complex, where fountains of red hot materials (extending 2000 m outwards) were inferred after correction of a partially overexposed image [*McEwen et al.*, 2000]. These fountains have been successfully modeled as representing just such an optically dense particle cloud [*Wilson and Head*, 2001].

[9] The relationship between gas pressures and velocities describing the variation in kinetic energy resulting from a given amount of near-isothermal gas expansion [*Wilson*, 1980] is given by:

$$u_f^2/2 = u_i^2/2 + [(n\,Q\,T_i)/m]\ln(P_i/P_f) + (1 - n)/\sigma_1, \quad (2)$$

where u_f is the final velocity of the gas–magma mixture; u_i the initial velocity of the gas–magma mixture; P_f the final

pressure; P_i the initial pressure; T_i the initial temperature of the gas–magma mixture, which is assumed constant over the optically thick region; σ_1 the density of magma droplets; n the mass fraction of incorporated gaseous SO_2, Q the universal gas constant, and m the molecular weight of the gas.

[10] Pressure varies as a result of volume variations alone, because the temperature is assumed constant, at T_i, in this region. We therefore relate the gas pressure to the volume, and hence the density, using the perfect gas law. We also relate increasing radial distances from the vent with decreasing bulk densities and increasing velocities according to the expression:

$$R_f = R_i[(\beta_i\,u_i)/(\beta_f\,u_f)]^{1/2}, \quad (3)$$

where R_f is the final distance from the vent; R_i the initial distance from the vent; β_f the final bulk density and β_i the initial bulk density. This relationship is obtained from the general expression for the constant erupted mass flux, which is given by $M = (\beta\,u\,A)$, where, in our specific case, $A = (2\,\pi\,R^2)$, the surface area of the hemispherical envelope occupied by the erupting gas–magma mixture.

[11] The bulk density of the gas–magma mixture exiting the vent is given by:

$$\beta = [(n/\rho) + (1 - n)/\sigma_1]^{-1}, \quad (4)$$

where ρ is the density of the gas phase, a function of pressure and temperature, and σ_1, the density of the magma droplets, is taken as 2600 kg m^{-3}, a value appropriate to a liquid basaltic composition. The final expression for the mass flux is then:

$$M = [(n/\rho) + (1 - n)/\sigma_1]^{-1}u(2\,\pi\,R^2). \quad (5)$$

[12] We next define the opacity depth of the Pillan and Pele volcanic plumes. This represents the radial extent of the plume through which radiation can partly penetrate because the plume is neither completely opaque nor optically thin. The general expression for the opacity depth Λ of a particle–gas mixture [*Wilson and Keil*, 1997] is given by:

$$\Lambda = 4\,S^3/G\,\pi\,\phi^2, \quad (6)$$

where S is the mean spacing between magma droplets/pyroclasts, ϕ is the mean diameter of droplets/pyroclasts, and G is a correction factor to account for the fact that a range of droplet sizes is probably present within eruption plumes. The optically thick region is unresolvable with current imagery and, as a consequence, we cannot exclude the possibility of a wide range of droplet sizes. *Wilson and Head* [1981b] modeled the lunar volcanic droplet size distribution using a logarithmic law. We adopt $\phi = 10\,\mu m$ as our initial estimate of the mean droplet size (and will show later that this is a reasonable assumption) and take G as 1.5, which implies that magmatic droplets can range between 1 and 100 μm in diameter (see derivation by *Wilson and Keil* [1997]). The very small sizes would result

from efficient melt disruption, similar to that which occurred on the Moon in eruptions into a vacuum [*Wilson and Head*, 1981b], and the low terminal fall velocity of the pyroclasts would cause them to be carried initially at essentially the same speed as the expanding and accelerating gas. Also, magma–SO_2 interactions would be expected to enhance the disruption process. The assumed droplet/pyroclast sizes are bigger by a factor of 100 than those inferred at the uppermost portions of the Pillan and Pele plumes through both Galileo and HST observations [*McEwen et al.*, 1997a; *Spencer et al.*, 1997a, 1997b]. Eruptions of gas and magma droplets in a near-vacuum environment would probably contribute to making magmatic droplets smaller, as a result of a greater gas expansion once the erupted mixture exits the volcanic vent. We demonstrate later the consequences of assuming other droplet sizes.

[13] No temperature, pressure, or density terms appear in equation (6). For our purpose we need an equation in which at least one of these terms is involved. The volume of a single magmatic droplet is given by $[(4/3)\pi(\phi/2)^3] = [(\pi\phi^3)/6]$. The number density of magma particles within the volcanic plume can be found from:

$$(1 - n)\beta = (1/S^3)\left[(\pi \phi^3)/6\right]\sigma_1. \tag{7}$$

The left side of this equation is the is the ratio of the total mass of magma to the total volume of magma plus gas. The right side is the same ratio expressed in terms of the mass of a single droplet, $[(\pi\phi^3)/6]\sigma_1$, and the average volume, S^3, occupied by that droplet. Substituting the expression for the bulk density of the gas–magma mixture into equation (7) we obtain:

$$S^3 = \left[((\pi \phi^3)/6)\sigma_1\right][(n/\rho) + (1 - n)/\sigma_1](1 - n)^{-1}. \tag{8}$$

Substituting this into the general expression for the opacity depth (equation (6)), we obtain for Λ:

$$\Lambda = \{(2 \phi \sigma_1)/[3 \ G(1 - n)]\}/[(n/\rho) + (1 - n)/\sigma_1]. \tag{9}$$

[14] In the calculations we introduce the term "opaque radius." This defines the extent of the completely opaque portion of the plume. We obtain it by subtracting the opacity depth value given by equation (6) from the radial extension of the optically thick zone outward from the vent.

[15] Within the optically thick portion of the plume, with increasing distances from the vent, gas densities and pressures continue to decrease until the flow regime changes and the classical treatment of particle–gas drag forces can no longer be applied [*Knudsen and Katz*, 1954]. This happens when the value of the mean free path λ of the gas molecules becomes similar to the mean magma droplet size. The mean free path λ is given by:

$$\lambda = (Q \ T_d)/(2 \ \pi \ d^2 \ N \ P_d), \tag{10}$$

where T_d is the temperature of the gas–magma mixture as particles start to decouple from the gas; P_d is the pressure of the mixture; d is the diameter of the gas molecules and N is Avogadro's number. Outward from the region where the gas–magma decoupling occurs, magma particles begin to pursue ballistic trajectories. We can calculate the velocity V_0

of the gas–magma mixture when the mean free path equals the mean droplet size in terms of the height of the plume:

$$V_0 = (2 \ g \ h_m)^{1/2}, \tag{11}$$

where g is the acceleration due to planetary gravity and h_m the average height reached by the Pillan and Pele plumes above the top of the optically thick region. The height of the Pillan plume ranged from 75 to 150 km (average value ~110 km) [*Spencer et al.*, 1997c; *Strom and Schneider*, 1982], whereas the Pele plume was 280–460 km high (average value ~350 km) in the Voyager and Galileo images. By substituting these two values into (17), we get mean velocity values, V_0, of ~600 and ~1100 m s^{-1} at Pillan and Pele, respectively.

2.4. The Optically Thin Portions of the Plumes

[16] When the mixture ceases to be optically thick, radiative cooling begins and subsequently both the temperature and pressure decrease adiabatically, still being linked to the radial expansion through the continuity requirement. As soon as the mean free path of the gas molecules exceeds the mean particle size, the pyroclasts will decouple from the gas to pursue essentially ballistic trajectories [*Wilson and Keil*, 1997] back to the surface, at some maximum range. Within this portion of the plume, temperatures, pressures, and densities of the expanding gas vary in accordance with an adiabatic law, and energy conservation provides final gas velocities as a function of pressure variations [*Wilson*, 1980]. The expression giving the kinetic energy resulting from a given amount of adiabatic gas expansion is:

$$u_f^2/2 = u_i^2/2 + [(n \ Q \ T_i)/m][\gamma/(\gamma - 1)]\left[1 - (P_f/P_i)^{[\gamma/(\gamma-1)]}\right], \tag{12}$$

where u_f is the final gas velocity, u_i is the initial gas velocity, P_f is the final gas pressure, P_i is the initial gas pressure, T_i is the initial gas temperature, n is the mass fraction of incorporated liquid SO_2, m is the molecular weight of SO_2 gas, γ is the specific heat ratio of SO_2 gas, and Q is the universal gas constant. We cannot use equation (12) directly in the model because our analysis starts from temperature variations, whereas only pressure variations can be estimated from this expression. We need to find an expression equivalent to the former, where temperatures are related to gas velocities. To do this, we combine the perfect gas law with the additional requirement for adiabatic gas expansion:

$$P/\rho^\gamma = \text{constant} \tag{13}$$

to get:

$$(P_f/P_i)^{[(\gamma-1)/\gamma]} = (T_f/T_i). \tag{14}$$

Hence, equation (12) can also be expressed as:

$$u_f^2/2 = u_i^2/2 + [(n \ Q \ T_i)/m][\gamma/(\gamma - 1)][1 - (T_f/T_i)], \tag{15}$$

where T_f is the final temperature, T_i is the initial temperature, u_f is the final velocity, u_i is the initial velocity,

and n the mass fraction of incorporated liquid SO_2. This represents the new relationship between gas temperatures and velocities, valid in the adiabatic case. The formula allowing calculation of the radial distance from the vent is the same as that used in the previous case (equation (3)) and so we can now follow the decrease in gas pressure, temperature and density with increasing radial distance from the vent until we reach the conditions under which solid SO_2 begins to form.

2.5. The Operation of the Numerical Model

[17] In the previous sections we have described the physical processes occurring as volcanic materials leave the vent and travel out to the distance at which solid SO_2 formation commences. However, the implementation of the model most conveniently involves the reverse of this sequence, starting the solution at the observed radial distances from the Pele and Pillan vents at which solid SO_2 first forms, as evidenced by the presence of surface frost.

[18] First, the pressure and the temperature at which solid SO_2 is expected to form on the Ionian surface are identified. The surface temperature is taken as 110 K, the diurnal average value, because temperatures on Io appear to range between 85 K (nighttime) and 130 K (daytime) [*Belton et al.*, 1996]. Thermodynamic data show that, at 110 K, SO_2 forms a solid condensate if the pressure is close to 10^{-4} Pa [*Kieffer*, 1982; *Kieffer et al.*, 2000]. Starting from this temperature and pressure, and increasing the temperature in 50 K steps, conditions are followed from the outer edges of the Pillan and Pele plumes inward toward the vent, using the various physical relationships outlined in the previous sections. As the radial distance from the vent decreases, the temperature, pressure and density of the gas–magma mixture increase and the velocity decreases. The process is terminated when the temperature approaches 1400 K at Pele or 1500 K at Pillan (the highest temperatures yet inferred for these vents on Io [*McEwen et al.*, 1998a, 1998b; *Davies et al.*, 2001]).

[19] Once the SO_2 condensation temperature and pressure conditions have been fixed, the adjustable parameters of the model are the mass flux from the vent, the mass fraction of SO_2 in the erupting magma–volatile mixture, the distance from the vent at which SO_2 is first observed on the surface, and the clast velocity at the point where gas and clasts decouple: ~600 m s^{-1} at Pillan and ~1100 m s^{-1} at Pele as judged by the plume heights. A very wide range of mass fluxes was investigated, and volatile fractions ranging from low magmatic values (<1 mass %) to values representing extreme mixing with near-vent nonjuvenile volatiles (>50 mass %) were explored. The distances from the vents at which SO_2 begins to be deposited were selected on the basis of the following arguments.

[20] The Pele deposit has been consistently observed to extend radially outward from the vent up to 550 km [*Strom and Schneider*, 1982; *McEwen et al.*, 2000], and bright annuli of SO_2 frost appear to surround the volcanic center at a comparable distance, ~500 km, from the central volcano. However, this cannot exclude the possibility of smaller amounts of SO_2 coverage, unresolvable in current imagery, at smaller distances from the vent [*Carlson et al.*, 1997], and we take 250 km as a generous lower limit.
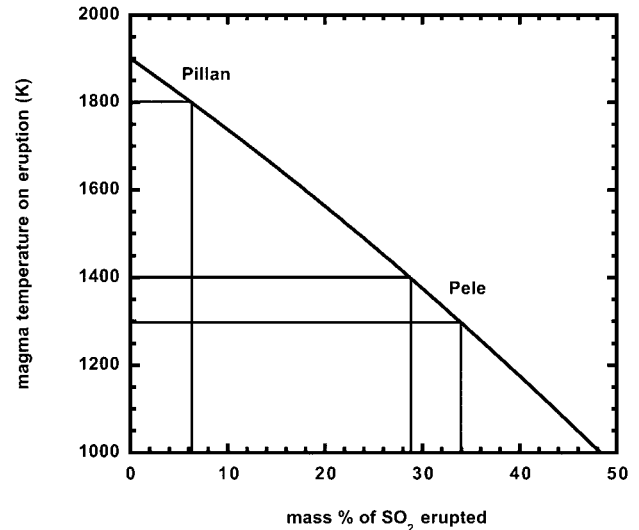
Figure 2. The eruption temperatures resulting from mixing of mantle magma at 1900 K with various mass percentages of SO_2 liquid derived from crustal aquifers. The two pairs of horizontal lines indicate the ranges of eruption temperatures inferred from Galileo thermal data. The corresponding pair of vertical lines indicates the implied SO_2 contents of the materials erupted at Pillan and Pele.

[21] There is much more uncertainty in the case of Pillan about the radial distance from the vent at which SO_2 deposition begins. The maximum range of dark (at all wavelengths) deposits at Pillan is ~200 km (see Figures 1a and 1b) [*McEwen et al.*, 1998a] and we take this to be the maximum range of ballistic pyroclasts which have escaped being coated with SO_2. Rather than using this value alone as the distance of initial deposition, we chose to use a fairly wide range of values, specifically 150–250 km, to assess the consequences of this uncertainty.

[22] In summary, the entire range of SO_2 solid formation distances seen or inferred at various times at Pillan and Pele can be simulated by using the values 150 and 250 for Pillan and 250 and 500 km for Pele.

3. Results
3.1. Eruption Conditions at the Pillan and Pele Volcanoes

[23] The interaction between magma and liquid SO_2 at shallow depths leads to a large difference between the temperature of the magma rising from the mantle and the magma temperature on eruption. As the amount of incorporated SO_2 ranges from 5 to 40 mass %, eruption temperatures range from 1810 to 1065 K if the magma temperature in the mantle is 1900 K: see Figure 2. If the mantle magma temperature were as high as 2100 K, corresponding eruption temperatures would range from 2010 to 1700 K. Based on a survey of the various available temperature estimates for the Pillan and Pele sites [*McEwen et al.*, 1998b, 2000; *Davies et al.*, 1999], we adopt vent temperatures in the range 1800–1900 K for Pillan and 1300–1400 K for Pele, and assume that the mantle magma temperature is 1900 K. The implied gas mass proportions
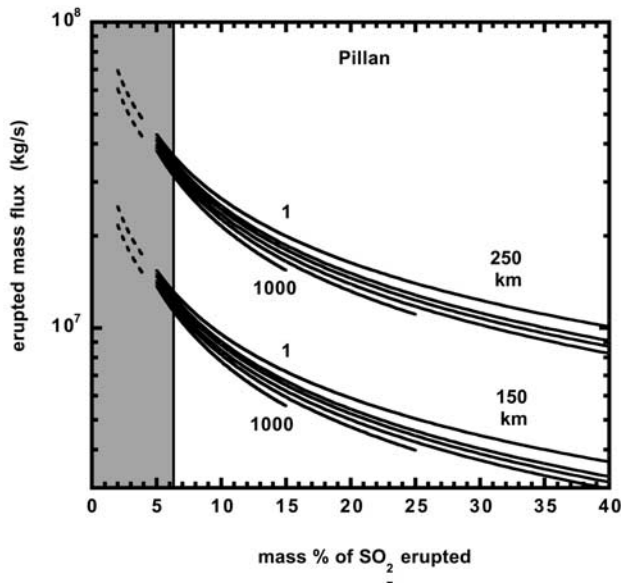
Figure 3. The erupted mass flux calculated for Pillan corresponding to a given SO_2 content in the erupted material. Values are given for two possible distances (150 and 250 km) from the vent at which SO_2 is first deposited as a solid on the surface and for mean pyroclast sizes of 1, 10, 30, 100, 300, and 1000 μm in each case. The curves for 1 and 1000 μm are indicated. The shaded region indicates the range of SO_2 mass fractions predicted from the range of eruption temperatures in Figure 2.

then range from a very small value up to ~6 % at Pillan and from ~29% to 34% at Pele.

[24] The combinations of erupted magma mass fluxes and amounts of incorporated near-surface SO_2 modeled to produce deposits comparable to those from the Pillan and Pele eruption sites are shown in Figures 3 and 4, respectively. On each of these figures, a series of curves is shown for mean pyroclast sizes ranging from 1 to 1000 μm; also, the ranges of gas mass fractions consistent with the adopted temperatures are indicated by the shaded region. The implications are that at Pillan, the erupted mass flux lies between $\sim 1 \times 10^7$ and $\sim 3 \times 10^7$ kg s^{-1} if the condensation distance is 150 km and between $\sim 3 \times 10^7$ and $\sim 10^8$ kg s^{-1} if the condensation distance is 250 km. Based on our arguments in section 2.5, we think that the latter distance is more commonly relevant than the former, and conclude that the average effusion rate probably lies within a factor of ~two of 5×10^7 kg s^{-1}. In the case of Pele the range of eruption rates is $(1.2-1.7) \times 10^7$ kg s^{-1} if the condensation distance is 250 km and $(4.5-6) \times 10^7$ kg s^{-1} if the condensation distance is 500 km. Again the latter value seems to be the more consistent with the observations discussed in section 2.5 and so we conclude that the average mass eruption rate lies within perhaps 30% of 5×10^7 kg s^{-1}. It is extremely interesting that, despite the great difference in implied amounts of incorporated SO_2, both of these eruption sites appear to have similar mass eruption rates.

[25] A classic problem in analyzing eruptions on Io is the uncertainty as to just how the decompression of the gas component occurs over the last few hundreds of meters of rise of the volcanic fluid to the surface [Kieffer, 1982].

Linked to this is the issue of whether the stream of gas and entrained pyroclasts is pressure balanced, which would require a sufficiently rapid outward flaring of the vent, or is choked, i.e., limited to the local sound speed when the vent is not sufficiently flared. In the latter case a series of shock waves would be generated immediately above the vent in order to decompress the flow [Kieffer, 1984; Kieffer and Sturtevant, 1984]. In our model, we follow the variation of conditions as gas and pyroclasts expand into a hemisphere centered on a point-source vent, working from the outer edge of the system inward. We are therefore able to specify a linked series of values of increasing pressure, decreasing mean pyroclast speed, increasing local sound speed and decreasing radial distance as the vent is approached, but we have no a priori way of deciding which pressure corresponds to the surface vent.

[26] Figures 5 and 6 show the variation of eruption speed in the vent with the assumed pressure in the vent and the assumed mean pyroclast size for Pillan and Pele, respectively. In each case the upper axis shows the depth which would correspond to the pressure on the lower axis if this were the lithostatic pressure, and curves are given for a range of possible mean pyroclast sizes. The plotted values correspond to an SO_2 mass fraction of 5% in the case of Pillan and 30% in the case of Pele, these being representative values implied by Figure 2. If we now assume that the pressure at a given radial distance from the vent is in fact the pressure in the vent, then that radial distance becomes the estimate of the vent radius. Figure 7 shows the resulting variation of vent radius with pressure. The results for both eruption sites are conveniently plotted on the same graph
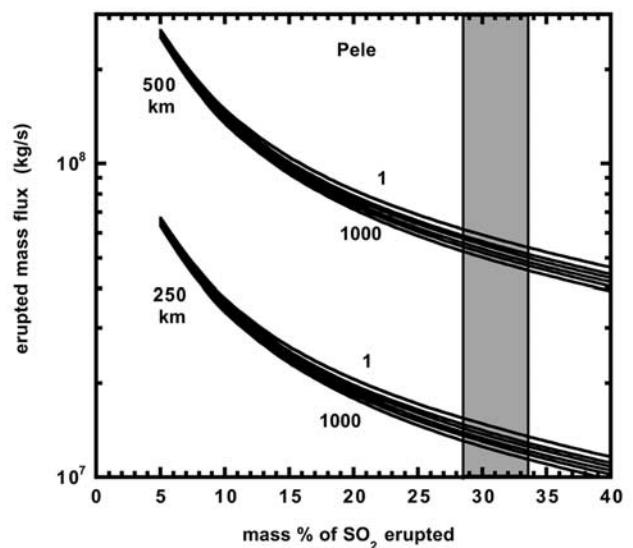
Figure 4. The erupted mass flux calculated for Pele corresponding to a given SO_2 content in the erupted material. Values are given for two possible distances (250 and 500 km) from the vent at which SO_2 is first deposited as a solid on the surface and for a range of mean pyroclast sizes of 1, 10, 30, 100, 300, and 1000 μm in each case. The curves for 1 and 1000 μm are indicated. The shaded region indicates the range of SO_2 mass fractions predicted from the range of eruption temperatures in Figure 2.
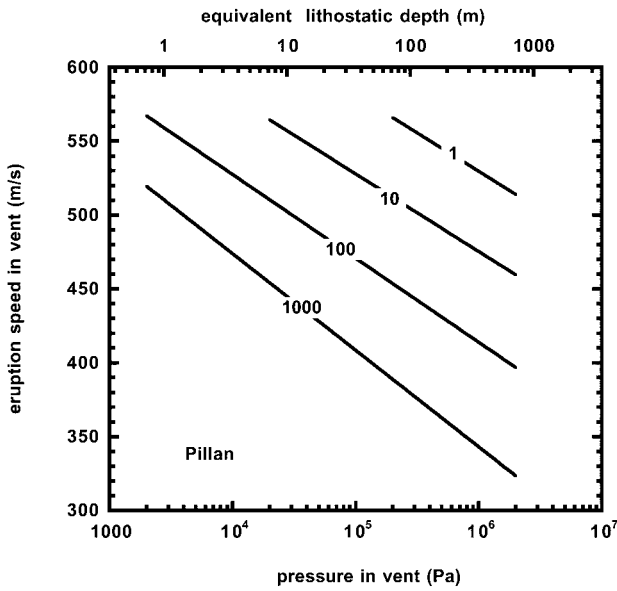
Figure 5. The eruption speeds of gas and pyroclasts leaving the Pillan vent as a function of the gas pressure in the vent for the range of mean pyroclast sizes indicated. The depths beneath the surface vent at which the lithostatic pressure would be equal to the gas pressure are indicated along the upper axis.

because there is only a very weak dependence of the vent radius on assumed mean pyroclast size.

[27] Finally, Figures 8 and 9 show the variation of Mach number with assumed vent pressure for Pillan and Pele, respectively. In these cases there is a significant dependence
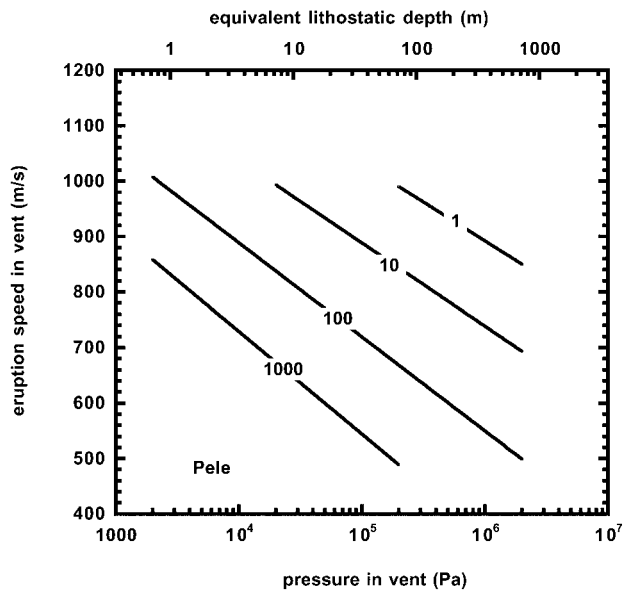
Figure 6. The eruption speeds of gas and pyroclasts leaving the Pele vent as a function of the gas pressure in the vent for the range of mean pyroclast sizes indicated. The depths beneath the surface vent at which the lithostatic pressure would be equal to the gas pressure are indicated along the upper axis.
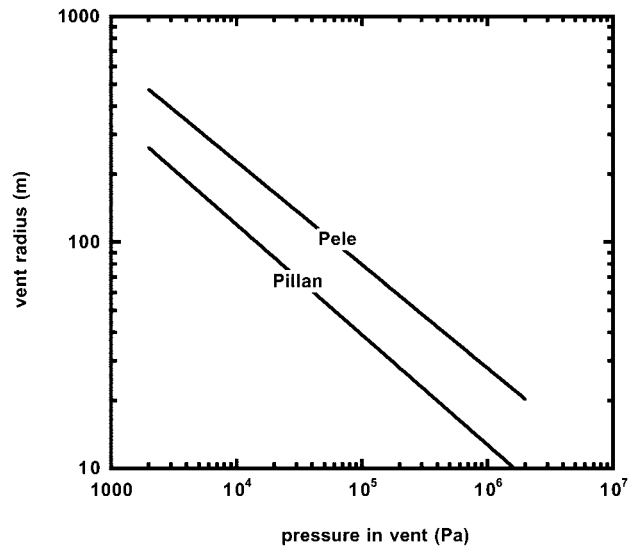
Figure 7. The radii of the surface vents for Pillan and Pele as a function of the pressure in the gas exiting the vent.

on mean pyroclast size, as shown. Note that, for the range of pressures considered, all of the Mach numbers are greater than unity, i.e., the flows are supersonic. This implies that we must interpret the vent radius values in Figure 7 rather carefully: the values correspond to the half widths of the erupting volcanic jets after they have passed through a subsonic to supersonic transition, whether this has happened beneath the surface, if the vent is sufficiently flared, or at the surface, if the eruption is choked.

3.2. The Extent of the Optically Thick Portions of the Plumes

[28] Figure 10 shows the radial extents of the optically thick zones of the Pillan and Pele plumes, respectively, as a
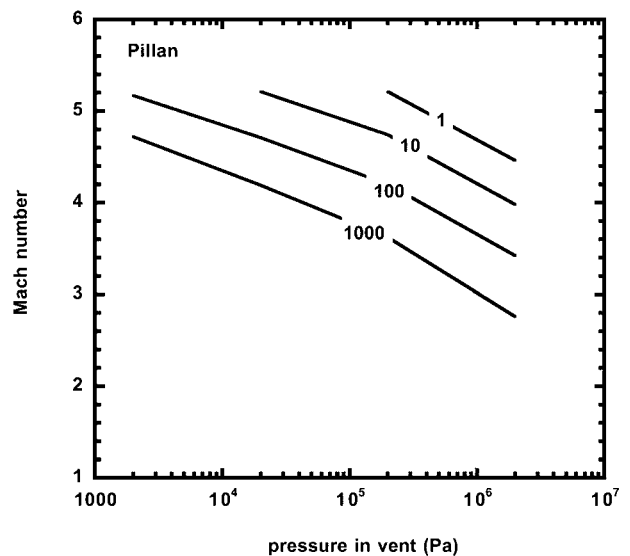
Figure 8. Internal Mach number of the stream of gas and pyroclasts exiting the Pillan vent as a function of the pressure in the gas and the mean pyroclast size (curves labeled in μm).
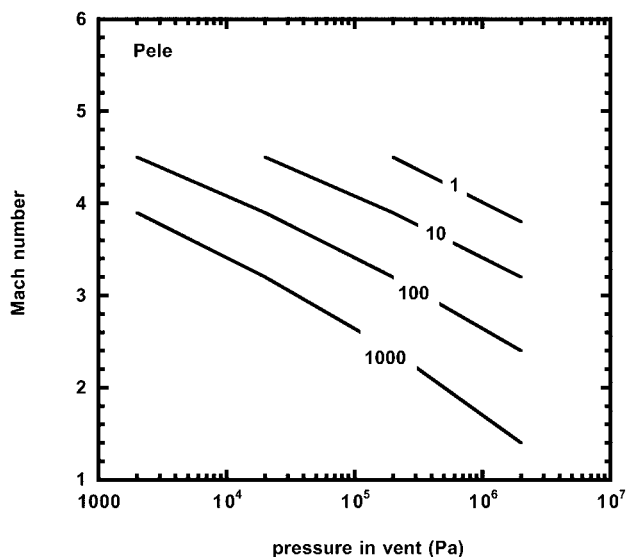
Figure 9. Internal Mach number of the stream of gas and pyroclasts exiting the Pele vent as a function of the pressure in the gas and the mean pyroclast size (curves labeled in μm).

function of mean pyroclast size. In each case a representative gas mass proportion in the erupting mixture is used based on Figure 2, up to 6% for Pillan and 29–34% for Pele. The extents of the optically thick regions are seen to increase with increasing distance from the vent at which condensation is taken to occur and to decrease at large mean clast sizes. The latter effect is to be expected because, at any given mass flux, an increase in mean particle size implies a reduction in particle number density. We note that the largest estimates of the radii of the optically thick regions, ~5 and 12 km for Pillan and Pele, respectively, correspond to structures with widths just less than one pixel and slightly more than 3 pixels at the resolutions of Figures 1a and 1b, respectively.

[29] Gas velocities at the edge of the optically thick region range between a minimum of 629 m s^{-1} at Pillan (for 5 mass % SO$_2$ and a mean pyroclast diameter of 1 mm) and a maximum of 1583 m s^{-1} at Pele (for 40 mass % SO$_2$ and a mean pyroclast diameter of 1 μm). These velocity values do not depend on the distance at which the onset of SO$_2$ deposition is taken to occur on the ground. We find that the decoupling between gas and magma droplets/pyroclasts always occurs well inside the boundary of the optically thick region.

[30] The radial distance from the vent at which decoupling occurs depends on the value chosen for the vent pressure (cf. Figure 7). At Pillan, if the vent pressure is taken as 20 kPa, decoupling occurs at 44 m from the vent for a mean pyroclast diameter of 1 μm and the pressure at decoupling is 3 kPa; in contrast, if the vent pressure is taken as 2 kPa, decoupling occurs at 2500 m from the vent for 1 mm diameter pyroclasts at a pressure of 30 Pa. At Pele an assumed vent pressure of 2 MPa leads to a decoupling distance of 72 m and decoupling pressure of 2 × 10^5 Pa for 1 μm diameter clasts, and a vent pressure of 2 kPa leads to a decoupling distance of 3900 m and decoupling pressure

of 25 Pa for 1 mm diameter clasts. Decoupling distances are not a function of the gas mass proportion within the erupting mixture but vary in direct proportion to the distance at which SO$_2$ condensation occurs on the ground. Thus the decoupling distance is subject to a much larger uncertainty than the radial extension of the optically thick region. The pressure at the point of decoupling varies inversely with the gas mass proportion within the magma but is not a function of the distance at which SO$_2$ deposition on the ground begins.

3.3. The Optically Thin Portions of the Plumes

[31] The fact that pyroclasts and gas are always found to enter the Knudsen regime and become decoupled before the optically thin parts of the plumes are reached simplifies the description of this region. Outside the optically thick region, clasts will cool to ambient temperature very rapidly: the time τ needed for a thermal wave to travel from the edge to the center of a spherical pyroclast of diameter φ is given by [*Carslaw and Jaeger*, 1947; *Thomas and Sparks*, 1992]

$$\tau = \phi^2/(8\,\kappa), \qquad (16)$$

where κ is the thermal diffusivity of rock (~10^{-6} m^2 s^{-1}). The time taken for a 1 mm diameter particle to relax thermally to equilibrium with its surroundings is thus less than 1 s, and even less time is needed for the smaller particles which we think are produced in these eruptions. The typical "airborne" travel times for pyroclasts erupted at Pillan and Pele are ~750 and 1050 s, respectively, and we conclude that the particles stay in approximate thermodynamic equilibrium with the gas. The maximum ballistic range is ~200 km at Pillan, less than the ~250 km distance
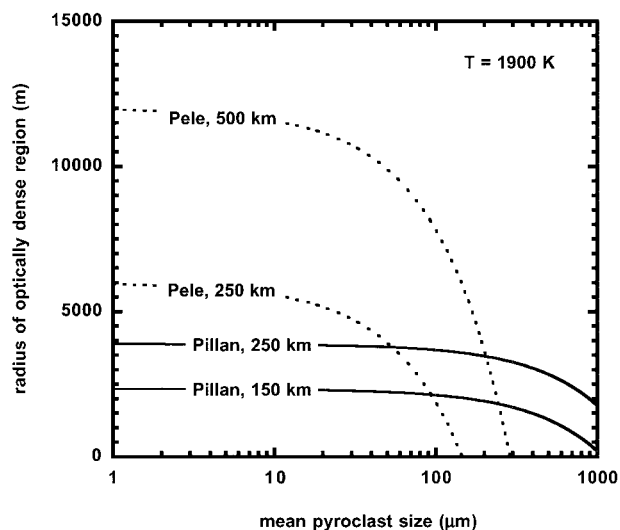
Figure 10. The radius of the optically dense, isothermal region above the vent as a function of mean pyroclast size when the temperature of the magma prior to interacting with near-surface SO$_2$ liquid is 1900 K. Values are shown, for both Pillan and Pele, for each of the two assumed distances (150 and 250 km and 250 and 500 km, respectively) from the vent at which SO$_2$ is first deposited as a solid on the surface.
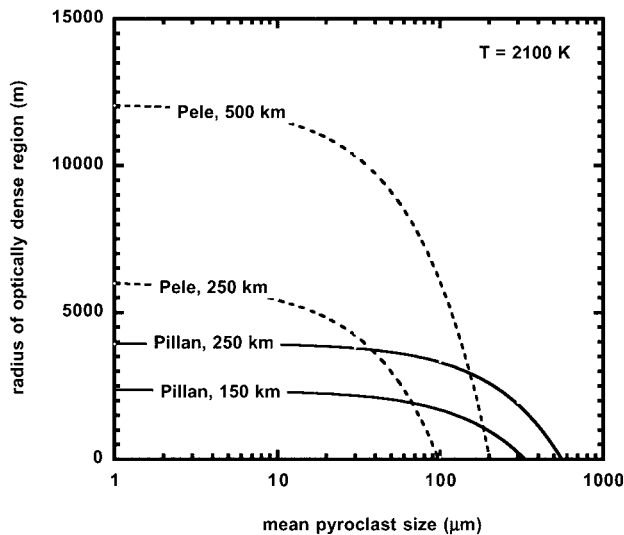
Figure 11. The radius of the optically dense, isothermal region above the vent as a function of mean pyroclast size when the temperature of the magma prior to interacting with near-surface SO_2 liquid is 2100 K. Values are shown, for both Pillan and Pele, for each of the two assumed distances (150 and 250 km, and 250 and 500 km, respectively) from the vent at which SO_2 is first deposited as a solid on the surface.

we have adopted as typical of SO_2 deposition onto the surface, whereas the ballistic range is ~670 km at Pele, significantly greater than the 500 km distance adopted for SO_2 deposition. However, the maximum heights reached by pyroclasts are 100 km at Pillan and 335 km at Pele. Thus in neither case is an SO_2 coating likely to form on particles that reach the ground within the radial distance at which direct deposition of SO_2 onto the surface takes place.

3.4. Constraints on Pyroclast Sizes

[32] Figure 10 shows that no optically dense region at high temperature can exist unless the mean pyroclast size is less than some critical value. The critical size implied for the Pele plume is in the range 150–300 μm, consistent with our expectations based on the submillimeter sizes of lunar pyroclast, whereas the critical size for eruptions at Pillan is much larger, well in excess of 1000 μm. We have investigated the dependence of this implied maximum pyroclast size on the various parameters of the model and find that if we increase the value that we assume for the magma temperature, so that a given eruption temperature corresponds to a larger proportion of added nonjuvenile volatiles, this reduces the pyroclast size corresponding to a given opaque radius. Figure 11 shows the equivalent of Figure 10 for a magma temperature of 2100 K: the range of maximum clast sizes predicted for Pele is only slightly reduced into the diameter range 100–200 μm, but the diameter range for Pillan is now much more plausible at 320–550 μm.

[33] The results in Figures 10 and 11 provide a possible mechanism of constraining the mean pyroclast sizes and eruption conditions even more closely. The target eruption temperatures used earlier in our calculations were derived from the work of *McEwen et al.* [1998b] and *Davies et al.*

[1999] who fitted two- and three-component model heat sources to Galileo thermal measurements. In addition to the temperatures of the source components, their models provided estimates of the area of the source component radiating at a given temperature. For the hottest component, which we have identified with the optically dense fire fountain, they found areas of 0.03 km^2 at Pillan and 0.575 km^2 at Pele. We have used our model values for vent radii (see Figure 7) to derive equivalent vent areas when viewed from above. These, like the radii, are functions of the assumed pressure in the vent, the mean particle size, and the distance from the vent at which SO_2 deposition on the ground begins.

[34] Figures 12 and 13 show the results, for Pillan and Pele respectively, for a magma temperature of 1900 K. The predicted surface area of the vent changes only slightly with mean pyroclast size but dramatically with assumed vent pressure. Thus we can only improve slightly on our maximum pyroclast size estimates, but we can constrain the pressure in the vent quite well. The implications are that at Pillan the vent pressure is within a factor of ~3 of 20 kPa and at Pele is within a factor of ~3 of 2 kPa. These pressures correspond to the lithostatic pressure on Io at depths of ~0.5 and 5 m, respectively, and support the idea that these eruptions were nearly pressure balanced rather than being choked. The best estimate of the mean pyroclast size for our preferred SO_2 deposition distance of 150 km at Pillan is ~10 μm, but increasing the deposition distance to 250 km would increase the size to 200–300 μm. For Pele, our preferred deposition distance of 250 km also implies a mean pyroclast size of ~10 μm. Increasing the deposition distance to 500 km for Pele would increase the size to very much more than 1000 μm, clearly not in accord with the maximum size deduced earlier. This apparent conflict is due
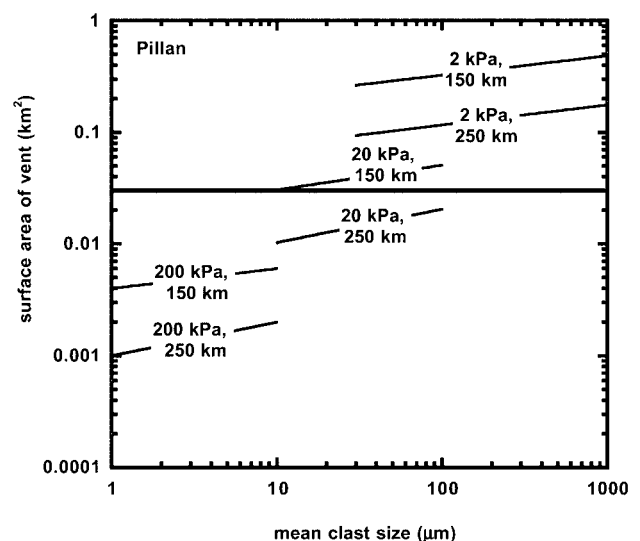
Figure 12. The surface area seen from above of the high-temperature vent structure at Pillan as a function of the assumed mean pyroclast size, the gas pressure in the vent, and the distance from the vent at which SO_2 is first deposited as a solid on the surface. The bold horizontal line indicates the surface area deduced from Galileo observations.
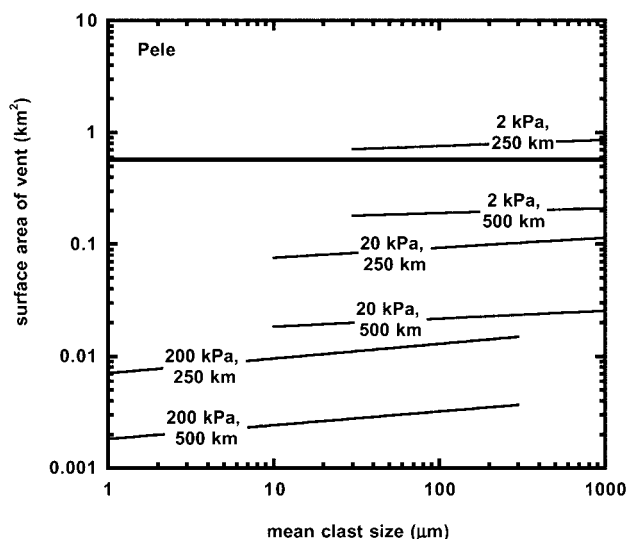
Figure 13. The surface area seen from above of the high-temperature vent structure at Pele as a function of the assumed mean pyroclast size, the gas pressure in the vent, and the distance from the vent at which SO_2 is first deposited as a solid on the surface. The bold horizontal line indicates the surface area deduced from Galileo observations.

to the maximum clast sizes being deduced from the radial extent of the optically dense region (on the assumption that this region lies entirely outside the vent), whereas the mean values are obtained from the vent area. We do not consider it likely that the mixture of clasts and gas erupting through the vent itself will have suffered significant cooling, even if the number density of clasts implies that it is not optically dense, because the walls of the conduit system will themselves be at the magmatic temperature. However, because we do not take explicit account of the presence of the conduit walls in the model, some of the model solutions can essentially correspond to situations where all of the optically dense region is underground.

4. Discussion

[35] There are various issues with which we have not dealt in detail. The first is the fate of pyroclasts ejected nearly vertically from the vent. After an initial phase in which both the rising clasts and the surrounding gas undergo cooling, the clasts fall back through the optically dense part of the plume and their surfaces are reheated. These particles may collide both with other pyroclasts and with gas molecules under conditions in which finite drag forces between gas and clasts exist, thus modifying the motions of all components of the system. We have neglected the influence of these clasts on both the temperature and the radial flow of the expanding gas on the grounds that the effects are not likely to be large; they should, however, be included in any more detailed model.

[36] Other issues which we have not explored in detail are the gas expansion rates and the gas and particle velocity distributions near the vent. Instead, we have tracked the pressure and velocity changes inward radially from the

outer edge of the system until a specified vent temperature is reached, and taken the radial distance from the surface at which this occurs as an index of the vent size. Although this probably gives at least an order of magnitude indication of the vent conditions, it neglects any system of shocks in and above the vent [*Kieffer*, 1982, 1984] which controls the subsonic to supersonic expansion and the range of angles from the vertical at which gas and pyroclasts are launched. These initial velocity vectors can exert a significant influence on the subsequent pattern of clast dispersion [*Wilson and Head*, 1981a; *Strom and Schneider*, 1982; *Glaze and Baloga*, 2000] and would also need to be incorporated in any elaboration of the model described here.

[37] Finally, we have developed our model on the assumption that eruptions take place from central vents rather than elongate fissures. The fortuitous observation of a fissure eruption in the Tvashtar Catena region [*McEwen et al.*, 2000] suggests that we need to extend the present work to incorporate variable vent geometry; *Wilson and Head* [2001] have made an attempt to address some of the issues involved in doing this.

5. Summary

[38] We have described a relatively simple model of eruption plumes on Io which provides estimates of the most important eruption parameters at both the Pillan and Pele volcanic centers. The main results are:

1. For the Pillan plume, the erupted magma mass flux probably lies within a factor of 2 of 5×10^7 kg s^{-1}. For the Pele plume the eruption rate probably lies within ~30% of 5×10^7 kg s^{-1}. These values are remarkably similar. The deduced mass fluxes increase with increasing distance at which SO_2 is first deposited on the ground whereas they decrease with increasing gas mass proportions within the erupted mixture. They are independent of the value of the gas pressure in the vent. The order of magnitude of the deduced mass fluxes is the same as that inferred for some massive explosive eruptions on the Moon [*Wilson and Head*, 1981b] and is at the lower end of the range inferred by *Wilson and Head* [2001] for the recent Tvashtar Catena fissure eruption on Io.

2. Our model solutions imply that the erupting magma contains up to ~6 mass % (at Pillan) and 29–34 mass % (at Pele) of a volatile phase, assumed to be SO_2. These value are much larger than any plausible volatile contents of magmas leaving the mantle and we assume that they represent liquid SO_2 incorporated into the rising magma from shallow aquifers. The fact that the values are very different suggests significant spatial variability in the availability of SO_2 in the crust of Io.

3. The ~1200–1800 K eruption temperatures observed by the Galileo spacecraft [*McEwen et al.*, 1998a, 1998b] are consistent with the incorporation into erupting magmas of the amounts of SO_2 that we have deduced provided that the premixing temperatures are at least 1900 K, reinforcing the suggestion [*McEwen et al.*, 1998b] that Io's magmas are commonly ultramafic.

4. We are not able to place very strong constraints on the mean sizes of the erupted silicate pyroclasts. For both eruption sites the best mean diameter estimate is close to 10 μm, though values could range up to a few hundred

micrometers at Pele and several hundred micrometers at Pillan.

5. The radial extents from the vent of the optically dense portions of the plumes are inferred to be at most ~2.5 km at Pillan and 6 km at Pele. The inferred radial extent increases with both increasing gas mass proportions within the erupted mixture and increasing distances from the vent at which the onset of SO_2 condensation occurs on the ground. These optically dense region sizes are just below the reliable resolution limits of the current best images of these plumes.

6. The inferred vent radii are ~90 m at Pillan and 500 m at Pele. Inferred vent size is directly proportional to the radial distance from the vent at which SO_2 begins to deposit on the ground, and is inversely proportional to the square root of the pressure in the vent.

7. Our estimates of the gas pressures in the vents are quite well constrained, being ~20 kPa at Pillan and 2 kPa at Pele. For all combinations of vent pressure and inferred gas mass proportion within the erupting gas–pyroclast mixtures, eruption velocities are predicted to be supersonic at the vent, though they are only just so for the highest gas mass fraction estimates in the Pele plume.

Notation

A	surface area of hemisphere above vent $(2\pi R^2)$, m^2
C_m	specific heat of magma at constant volume, equal to 1100, $J\ kg^{-1}\ K^{-1}$
C_{sl}	specific heat of liquid SO_2 at constant volume, equal to 1300, $J\ kg^{-1}\ K^{-1}$
C_{sv}	specific heat of SO_2 vapor at constant volume, equal to 800, $J\ kg^{-1}\ K^{-1}$
D	radial distance from vent of SO_2 condensation, m
G	correction factor for range of pyroclast sizes, equal to 1.5
H	height in plume of SO_2 condensation, m
L_s	latent heat of vaporization of SO_2, equal to 4×10^5, $J\ kg^{-1}$
M	mass flux of erupting material, $kg\ s^{-1}$
N	Avogadro's number, equal to 6.02×10^{26}, $kmol^{-1}$
P_d	gas pressure when pyroclasts and gas decouple, Pa
P_f	final pressure of gas–magma mixture, Pa
P_i	initial pressure of gas–magma mixture, Pa
Q	universal gas constant, equal to 8.314, $kJ\ K^{-1}\ kmol^{-1}$
R	radial distance from vent, m
R_f	final radial distance from vent, m
R_i	initial radial distance from vent, m
S	mean spacing between pyroclasts, m
T	equilibrium temperature of magma–SO_2 mixture, K
T_b	temperature at which SO_2 evaporates, equal to 262.4, K
T_d	temperature when pyroclasts and gas decouple, K
T_i	initial temperature of the gas–magma mixture, K
T_l	initial SO_2 liquid temperature, equal to 200, K
T_{mi}	initial magma temperature, K
V_0	velocity of pyroclasts decoupling from gas, $m\ s^{-1}$
d	diameter of SO_2 molecule, equal to 4×10^{-10}, m
g	acceleration due to gravity, equal to 1.8, $m\ s^{-2}$
h_m	plume top height above optically thick region, m
m	molecular weight of SO_2
n	mass fraction of SO_2 entrained into magma
u_f	final velocity of gas–magma mixture, $m\ s^{-1}$
u_i	initial velocity of the gas–magma mixture, $m\ s^{-1}$
Λ	opacity depth of particle–gas mixture, m
β	general bulk density of gas–pyroclast mixture, $kg\ m^{-3}$
β_f	final bulk density of gas–pyroclast mixture, $kg\ m^{-3}$
β_i	initial bulk density of gas–pyroclast mixture, $kg\ m^{-3}$
γ	ratio of specific heats for SO_2, equal to 1.33
θ	limiting angle for pyroclast ejection
κ	thermal diffusivity of rock, equal to 7×10^{-7}, $m^2\ s^{-1}$
λ	mean free path of molecules, m
ϕ	mean diameter of pyroclasts, m
ρ	density of gas phase, $kg\ m^{-3}$
σ	density of solid magma droplets, equal to 2900, $kg\ m^{-3}$
σ_l	density of liquid magma droplets, equal to 2600, $kg\ m^{-3}$
τ	time for passage of thermal wave, s

References

Ammann, M., and H. Burtscher, Aerosol dynamics and light-scattering properties of a volcanic plume, *J. Geophys. Res.*, *98*, 19,705–19,711, 1993.

Belton, M. J. S., Galileo first images of Jupiter and the Galilean satellites, *Science*, *274*, 377–385, 1996.

Butler, P., Volatile compounds in lunar glasses from the Apollo 15 and 17 lunar sites, *Proc. Lunar Sci. Conf. 9th, Geochim. Cosmochim. Acta Suppl.*, *10*, pp. 1459–1471, 1978.

Carlson, R. W., et al., The distribution of sulfur dioxide and other infrared absorbers on the surface of Io, *Geophys. Res. Lett.*, *24*, 2479–2483, 1997.

Carslaw, H. S., and J. C. Jaeger, *Conduction of Heat in Solids*, 386 pp., Oxford Univ. Press, New York, 1947.

Cataldo, V., and L. Wilson, Theoretical comparison between explosive volcanic eruptions issuing from circular and fissure vents on Io (abstract), *Lunar Planet. Sci.*, *XXXI*, 2000.

Chou, C., W. V. Boynton, L. L. Sundberg, and J. T. Wasson, Volatiles on the surface of Apollo 15 green glass and trace elements distributions among Apollo 15 soils, *Proc. Lunar Sci. Conf. 6th, Geochim. Cosmochim. Acta Suppl.*, *10*, pp. 1701–1727, 1975.

Collins, S. A., Spatial color variations in the volcanic plume at Loki, on Io, *J. Geophys. Res.*, *86*, 8621–8626, 1981.

Cook, A. F., E. M. Shoemaker, and B. A. Smith, Dynamics of volcanic plumes on Io, *Nature*, *280*, 743–746, 1979.

Davies, A. G., L. P. Keszthelyi, R. M. C. Lopes-Gautier, A. S. McEwen, W. D. Smithe, L. Soderblom, and R. W. Carlson, Thermal signature, eruption style and eruption evolution at Pele and Pillan Patera on Io (abstract), *Lunar Planet. Sci.*, *XXX*, CD-ROM, 1999.

Davies, A. G., et al., Thermal signature, eruption style, and eruption evolution at Pele and Pillan on Io, *J. Geophys. Res.*, *106*, 33,079–33,103, 2001.

Gibson, E. K., and C. B. Moore, Variable carbon contents of lunar soil 74220, *Earth Planet. Sci. Lett.*, *20*, 404, 1973a.

Gibson, E. K., and G. W. Moore, Carbon and sulfur distributions and abundances in lunar fines, *Proc. Lunar Sci. Conf. 4th, Geochim. Cosmochim. Acta Suppl.*, 4, pp. 1577–1586, 1973b.

Gilbert, J. S., and S. J. Lane, The origin of accretionary lapilli, *Bull. Volcanol.*, *56*, 398–411, 1994.

Glaze, L. S., and S. M. Baloga, Stochastic-ballistic eruption plumes on Io, *J. Geophys. Res.*, *105*, 17,579–17,588, 2000.

James, M. R., and L. Wilson, An optical model for ballistic plumes on Io (abstract), *Lunar Planet. Sci.*, *XXIX*, 1998.

Johnson, T. V., D. L. Matson, D. L. Blaney, G. J. Veeder, and A. G. Davies, Stealth plumes on Io, *Geophys. Res. Lett.*, *22*, 3293–3296, 1995.

Keszthelyi, L., and A. S. McEwen, Magmatic differentiation of Io, *Icarus*, *130*, 437–448, 1997.

Kieffer, S. W., Dynamics and Thermodynamics of volcanic eruptions: Implications for the plumes on Io, in *Satellites of Jupiter*, edited by D. Morrison, pp. 647–723, Univ. of Ariz. Press, Tucson, 1982.

Kieffer, S. W., Factors governing the structure of volcanic jets, in *Explosive Volcanism: Inception, Evolution and Hazards*, pp. 143–157, Natl. Acad. Sci. Press, Washington, D. C., 1984.

Kieffer, S. W., and B. Sturtevant, Laboratory studies of volcanic jets, *J. Geophys. Res.*, *89*, 8253–8268, 1984.

Kieffer, S. W., R. Lopes-Gautier, A. McEwen, W. Smythe, L. Keszthelyi,

and R. Carlson, Prometheus: Io's wandering plume, *Science*, *288*, 1204–1208, 2000.

Knudsen, J. G., and D. L. Katz, *Fluid Dynamics and Heat Transfer*, 243 pp., McGraw-Hill, New York, 1954.

Lellouche, E., Io's atmosphere: Not yet understood, *Icarus*, *124*, 1–21, 1996.

Lopes-Gautier, R., et al., A close-up look at Io from Galileo's near-infrared mapping spectrometer, *Science*, *288*, 1201–1204, 2000.

McEwen, A. S., and L. A. Soderblom, Two classes of volcanic plumes on Io, *Icarus*, *55*, 191–217, 1983.

McEwen, A. S., J. Spencer, D. Simonelli, T. Johnson, and L. Keszthelyi, Io plume observations from Galileo and HST, *Lunar Planet. Sci.*, *XXVIII*, 911–912, 1997a.

McEwen, A. S., D. Simonelli, D. R. Senske, K. P. Klaasen, L. Keszthelyi, T. V. Johnson, P. E. Geissler, M. H. Carr, and M. J. S. Belton, High-temperature hot spots on Io as seen by the Galileo solid state imaging (SSI) experiment, *Geophys. Res. Lett.*, *24*, 2443–2446, 1997b.

McEwen, A., et al., Active volcanism on Io as seen by Galileo SSI, *Icarus*, *135*, 181–219, 1998a.

McEwen, A. S., et al., High-temperature silicate volcanism on Jupiter's Moon Io, *Science*, *281*, 87–90, 1998b.

McEwen, A. S., et al., Galileo at Io: Results from high-resolution imaging, *Science*, *288*, 1193–1198, 2000.

Meyer, C., D. S. McKay, D. H. Anderson, and P. Butler, The source of sublimates on the Apollo green and Apollo 17 orange glass samples, *Proc. Lunar Sci. Conf. 6th, Geochim. Cosmochim. Acta Suppl.*, 6, pp. 1673–1699, 1975.

Rogers, R. R., and M. K. Yau, *A Short Course in Cloud Physics*, 293 pp., Pergamon, New York, 1989.

Smith, B. A., E. M. Shoemaker, S. W. Kieffer, and A. F. Cook, The role of SO_2 in volcanism on Io, *Nature*, *280*, 738–743, 1979.

Spencer, J. R., A. McEwen, P. Sartoretti, G. Ballester, M. McGrath, and D. Nash, Hubble Space Telescope observations of plumes and surface changes on Io, *Proc. Conf. on Io during the Galileo Era*, p. 47, Lowell Obs., Flagstaff, Ariz., 1997a.

Spencer, J. R., P. Sartoretti, G. E. Ballester, A. S. McEwen, J. T. Clarke, and M. A. McGrath, The Pele plume (Io): Observations with the Hubble Space Telescope, *Geophys. Res. Lett.*, *24*, 2471–2474, 1997b.

Spencer, J. R., J. A. Stansberry, C. Dumas, D. Vakil, R. Pregler, M. Hicks, and K. Hege, A history of high-temperature Io volcanism: February 1995 to May 1997, *Geophys. Res. Lett.*, *24*, 2451–2454, 1997c.

Spencer, J. R., K. L. Jessup, M. A. McGrath, G. E. Ballester, and R. Yelle, Discovery of gaseous S_2 in Io's Pele plume, *Science*, *288*, 1208–1210, 2000.

Strom R. G., and N. M. Schneider, Volcanic eruption plumes on Io, in *Satellites of Jupiter*, edited by D. Morrison, pp. 598–633, Univ. of Arizona Press, Tucson, Ariz., 1982.

Strom, R. G., J. R. Terrile, H. Masursky, and C. Hansen, Volcanic eruption plumes on Io, *Nature*, *280*, 733–736, 1979.

Thomas, R. M. E., and R. S. J. Sparks, Cooling of tephra during fallout from eruption columns, *Bull. Volcanol.*, *54*, 542–553, 1992.

Wasson, J. T., W. V. Boynton, G. W. Kallemeyn, L. L. Sundberg, and C. M. Wai, Volatile compounds released during lunar lava fountaining, *Proc. Lunar Sci. Conf. 7th, Geochim. Cosmochim. Acta Suppl.*, 7, pp. 1583–1595, 1976.

Wilson, L., Relationships between pressure, volatile content and ejecta velocity in three types of volcanic explosion, *J. Volcanol. Geotherm. Res.*, *8*, 297–313, 1980.

Wilson, L., and J. W. Head, Io volcanic eruptions: Mass eruption rate estimates (abstract), *Lunar Planet. Sci.*, *XII*, 1191–1193, 1981a.

Wilson, L., and J. W. Head, Ascent and eruption of basaltic magma on the Earth and Moon, *J. Geophys. Res.*, *86*, 2971–3001, 1981b.

Wilson, L., and J. W. Head, Lava fountains from a fissure eruption on Io: Implications for dike emplacement mechanisms, eruption rates and crustal structure, *J. Geophys. Res.*, *106*, 32,997–33,004, 2001.

Wilson, L., and K. Keil, The fate of pyroclasts produced in explosive eruptions on the asteroid 4 Vesta, *Meteorol. Planet. Sci.*, *32*, 813–823, 1997.

Wohletz, K. H., Explosive magma–water interactions: Thermodynamics, explosion mechanisms, and field studies, *Bull. Volcanol.*, *48*, 245–264, 1986.

————————

E. Cataldo, J. Gilbert, S. Lane, and L. Wilson, Department of Environmental Science, Institute of Environmental and Natural Sciences, Lancaster University, Lancaster LA1 4YQ, UK. (l.wilson@lancaster.uc.uk)